A universal free energy relationship for both hard and soft radical addition in water

Nolte, T.M.; Hendriks, A.J.; Novák, L.A.; Peijnenburg, W.J.G.M.

Received: 13 October 2021 | Revised: 20 December 2021 | Accepted: 28 December 2021

DOI: 10.1002/poc.4317

RESEARCH ARTICLE

Journal of Physical Organic Chemistry WILEY

A universal free energy relationship for both hard and soft radical addition in water

Tom M. Nolte[1] | **A. Jan Hendriks**[1] | **Laurie A. Novák**[1] | **Willie J. G. M. Peijnenburg**[2,3]

[1]Department of Environmental Science, Institute for Water and Wetland Research, Radboud University Nijmegen, Nijmegen, The Netherlands

[2]Department of Environmental Science, Institute for Water and Wetland Research, National Institute of Public Health and the Environment, Bilthoven, The Netherlands

[3]Institute of Environmental Sciences (CML), Leiden University, Leiden, The Netherlands

Correspondence
Tom M. Nolte, Department of Environmental Science, Institute for Water and Wetland Research, Radboud University Nijmegen, 6500 GL Nijmegen, The Netherlands.
Email: t.nolte@ru.nl; tom.m.nolte@gmail.com

Funding information
Dutch Research Council (NWO), Grant/Award Number: 15759

Abstract

Prioritization of (eco)toxicological risks and technological endpoints among 100,000+ potential substances, conditions and mechanisms requires computationally 'inexpensive' and accurate tools to 'screen' reactivity and identify reaction products. Such prediction tools are very scarce. Left unresolved, charge-transfer and hydration complicate predictions. Based on experimental reaction of radicals ($^3O_2$, $CH_3^{\bullet}$, $CO_3^{\bullet-}$ etc.) with organic substrates, we hypothesized that a universal linear free energy relationship (LFER) can rationalize these reactions to accurately predict addition rates.

We calculated free energies of forming charge-separated intermediates from explicit descriptions of addition reaction products. We combined these energies, via a thermodynamic cycle, with electron transfer energies to calculate product formation energies. All energies include consideration of hydration effects by water. We ascribe feasibilities of 'hard' (ionic) and 'soft' (covalent) mechanisms to the relevance of the charge-separated intermediate.

Analysis shows that activation energies effectively relate to a combination of product formation energies and charge-separation energies. The relative importance of these is determined by a mixing parameter, which is mostly constant for a given radical (substrate). Via the Eyring equation, our universal LFER explains up to 94% of the variance in data for rate constants. Prediction error is a factor 5 (2 SD), only slightly larger than variation in experimentation, particularly sensitive to varying reaction conditions.

Minimal parametrization ensures that our new framework for calculating reactivity of radical addition is accurate, robust and with satisfactory rational. Calculation time for 100 reactions is <1 h on a standard desktop PC. In anticipation of underpinning with an even wider range of reagents, this 'inexpensive' calculus can more easily assess a greater domain of structures and extrapolate to new structures. This helps to better assess and select favourable non-toxic, environmentally friendly and technologically superior chemical (sub)structures.

KEYWORDS
LFER, oxygen, radical addition

1 | INTRODUCTION

Upon release in certain environments, chemicals become subject to biotic and abiotic breakdown. Degradation mechanisms typically involve reactive species, produced in, for example, living cells, surface water and electrochemical systems.[1,2] 'Fate assessment' focuses on describing the reactivity of the 'parent' form of, mostly organic, chemicals.[3,4] After such substance's initial reactions, however, reaction products can participate in follow-up reactions with, for example, oxygen and organic matter (^{3}OM), which are ubiquitous in the environment.[5,6] The concentrations of such reactants determine the accumulation of chemicals in the environment and, ultimately, which chemicals require (chronic) toxicological evaluation. Thus, it is important to understand the mechanisms by which chemicals react by different pathways.

Experimentally determining chemical fate is generally expensive and time intensive, hence virtually impossible to perform in practice. With 100,000+ chemicals, reagents and reactions to be assessed,[7,8] we cannot quantify their rates in full experimental detail. Rather, we can reduce costs and increase the sample variation and throughput by supplementing experiments with computational methods.[9] This allows selecting 'problem' and 'priority' substances that require further study. Statisticians predict fate by (cor)relating reaction rate constants (k_r) to easily retrievable (automatically generated) topological, electrostatic and energetic descriptors. Prediction accuracies, however, are with mixed results depending on the reagents. Results may also not support interpretation in terms of reaction mechanisms, more so for complex molecular structures falling outside of the model's domain of applicability.

Alternatively, computational chemists and physicists apply 'ab initio' quantum chemical methods to calculate the free energy of activation, or energy of the transition state (TS), $\Delta G^{\ddagger}$, and apply the Eyring equation to estimate reaction rate constants:

$$k_r = \frac{kT}{h} \cdot q \cdot e^{\frac{-\Delta G^{\ddagger}}{R \cdot T}} \tag{1-1}$$

$$\Delta G^{\ddagger} \Psi_{TS}(r,t) = \widehat{H} \Psi_{TS}(r,t) \tag{1-2}$$

where $(kT/h) \cdot q$ is a pre-exponential frequency factor, $e^{-\Delta G^{\ddagger}/RT}$ the fraction of collisions having sufficient energy to react and Ψ_{TS} the wave function of the TS. The methods involve the exploration (via $\widehat{H}$) of free energy changes along the reaction coordinate (r,t). 'Precise' calculations (1) involve description of time-dependent three-dimensional interactions, which requires much computing for a full description, and (2) require specific ('appropriate') basis sets, which can sometimes prove unreliable,[10,11] hampering accuracy.

1.1 | Theory

Conveniently, electronic properties of the TS can be inferred from properties of the ground-state molecules. For a better and more efficient description of the TS, theoretical chemists also 'mix' (M) plausible configurations with the ground-state electronic configuration.[12] Using some assumptions, they write Ψ_{TS} as[13]

$$\Psi_{TS} \approx N\left\{\frac{1}{\sqrt{2}}\left(\Psi_{reactants}(r,t) + \Psi_{products}(r,t)\right) + \lambda_M \Phi_M(r,t)\right\} \tag{2}$$

wherein λ_M is a mixing coefficient for Φ_M describing the extent of the additional mixing and N a normalization constant. The parameter λ_M, however, is not easily accessible: Often, it needs to be acquired from experimentation or detailed simulation. This is not suitable when aiming for 'cheap' predictions.

The height of an energetic barrier is usually proportional to reaction exothermicity ('unperturbed' Bell–Evans–Polanyi-type relationship). Therefore, simplifications use static configurations for reactants or the TS, requiring foreknowledge on the reaction pathway. Product formation (PF) usually occurs via different and lengthier (spatial) movements or (re) orientations (r,t) as compared with those in the TS state (curve-crossing theory[14,15]). By analogy, we may assume that the contribution from mixing to $\Delta G^{\ddagger}$ is independent from that of PF. If we substitute Equation 2 in 1-2, and consider only the differences in activation energies between compounds by applying the linear free energy relationship (LFER) concept ($\Delta(\Delta G^{\ddagger})$ $\sigma\Delta(\Delta G)$),[14,16] we can separate the variables (t, r) to reformulate:

$$\lambda_M \approx \frac{\Delta\left(\Delta G^{\ddagger}\right) - \sigma_{PF}\Delta(\Delta G_{PF})}{\sigma_M \Delta(\Delta G_M)} F_c \quad (3)$$

with $F_c = \{\Psi_{reactants}(t_{PF}, r_{PF}) + \Psi_{products}(t_{PF}, r_{PF})\}/\{\Phi_M(t_M, r_M)\}$. σ_{PF} and σ_M are (Taft-like) substituent factors for similar reaction 'PF' and 'mixing' mechanisms, respectively.[17,18] ΔG_M is the free energy change associated with mixing, and ΔG_{PF} is the free energy change for PF. Equation 3 shows that the mixing coefficient λ_M is tied to substituent factors σ, spatial and temporal (r,t) configurations of the reactants, products and mixing species (Ψ and Φ), and the free energy changes ΔG_{PF} and ΔG_M.

One-electron oxidation of organic chemicals involves a σ_{PF} of approximately $10^{2.3}$ M^{-1} s^{-1} eV^{-1}, which does not vary significantly between reagents and similar reaction mechanisms $10^{\pm 0.2}$ M^{-1} s^{-1} eV^{-1}.[19,20] By extension, 'similar mixing mechanisms' entail constant σ_M.[20] In other words, these reactions entail similar rate-limiting steps, in terms of PF, mixing, or both. Experimental values for ΔG are widely available or are reasonably easy and inexpensive to compute.[19,21] This opens the door to quantify λ_M via information on ΔG_{RP} and ΔG_M (Equation 3). As compared with experimentation or detailed simulation, Equation 3 would straightforwardly determine λ_M values via 'cheap calculus'. Information on λ_M, in turn, will facilitate predicting $\Delta G^{\ddagger}$ (Equations 1 and 2).

1.2 | Hypothesis

To test Equation 3, we considered 'addition-type' reaction mechanisms. For these, configurations that contribute to mixing M are those corresponding to a thermodynamically relevant polar charge-separated (CS) complex[22] (Figure 1): For example, an electron can transfer from the donor (D) to acceptor (A) to generate a D^+A^- configuration, thereafter to delocalize into a charge-transferred (CT) product:

$$\Phi_M = \Phi_{CS} = D^+A^- \quad (4)$$

$$D\!:\ A^{\bullet} \ \rightarrow\ D^{+}\!:\ A\!:^{-} \ \rightarrow\ D^{\delta+}\!:\!:A^{\delta-}$$

We explain our stepwise method to obtain $\sigma\Delta(\Delta G)$ values for reaction, to determine λ_M and thereby to predict $\Delta G^{\ddagger}$ via energetics of reactants and products. The weak Lewis base triplet oxygen ($^3O_2$) and Lewis acid carbonate radical ($CO_3^{\bullet-}$) are of great environmental, biological and technological importance.[23,24] We therefore validate our method with data for addition-type reactions involving $^3O_2$, $CO_3^{\bullet-}$ as well as $CH_3^{\bullet}$, wherefore great variety in $\Delta G^{\ddagger}$ is known.[21] We demonstrate facile prediction of addition rate constants with satisfactory performance within a factor 5 accuracy (2 SD), circumventing 'costly' assessment. The discussion details the limits of the calculus and provides examples.

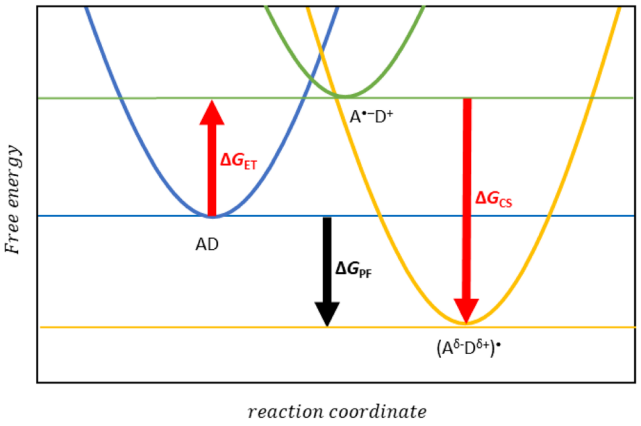

FIGURE 1 Reaction diagram with relative energy levels for the ground-state $\Psi_{(AD)}$ (blue), a mixing (M) intermediate CS-state $\Phi_{A^-D^+}$ (green) and product $\Psi_{(A^{\delta-}D^{\delta+}\cdot)}$ (yellow) configurations over the reaction coordinate (r,t)

2 | METHODS

Our goal was to circumvent 'costly' studies and determine λ_M via Equation 3 for CS species. We confined to computationally inexpensive methods as predictors. SI1 and SI2 detail quantum-chemical (PM7) calculations and theoretical underpinning. We obtained λ_M by comparing between the left- and right-hand terms, that is, obtain slopes of the regressions, of

$$\frac{F_c}{\lambda_M}\left(\Delta\left(\Delta G^{\ddagger}\right) - \sigma_{PF}\Delta(\Delta G_{PF})\right) \approx \sigma_{CS}\Delta(\Delta G_{CS}) \quad (5)$$

Stepwise, we obtained values for σ_{PF} and σ_{CS} from literature (Section 2.3) and different electronic configurations and molecular orbital calculations (Section 2.1.1). We evaluate F_c as approximately a constant factor for small organic molecules (Section 2.3).

We applied $\Delta\left(\Delta G^{\ddagger}\right)$ values to test our calculus (Equation 5) via experimental rate constants (k_R) and Eyring (Equation 1-1). We applied k_R for reactions R1, R2 and so forth (SI3):

$$\Delta_{1,2}\left(\Delta G^{\ddagger}\right) = \frac{q_{R1}}{q_{R2}} \ln\left(\frac{k_{R1}}{k_{R2}}\right) \quad (6)$$

wherein q values are frequency factors (Section 2.3). Thereby, $\Delta G^{\ddagger}$ data relate to one uniform site on each chemical. k_R values are addition(-type) reactions between $^3O_2$ and small organic substrates: aliphatic and aromatic radicals as well as singlet state molecules. For environmental/biological relevance, we only considered aqueous phase reactions and energies. SI3 details selection and (minor) curation of data, including those used for method validation ($CH_3^{\bullet}$, $CO_3^{\bullet -}$).

We thereby parametrize predictions for $\Delta G^{\ddagger}$ for new reactions on the basis of ΔG (Section 2.1). ΔG is the sum of energy changes resulting from the valence electron(s) going from one electronic state (e.g., $\Psi_{\text{reactants}} = \text{AD}$) to another (e.g., $\Psi_{\text{products}} = A^{\delta-}D^{\delta+\bullet}$) (Equations 3 and 4) and any associated change in electrostatic interaction between donor D, acceptor A and solvent. By combining frontier orbitals (FOs), electrostatic (E) and solvation (hydr) interaction, we calculate ΔG for both PF and CS[22,25] via

$$\Delta G = n\Delta G_{\text{FO}} + \delta\Delta G_{\text{E}} + \Delta G_{\text{hydr}} \quad (7)$$

wherein n is the number of electrons transferred between FOs, details in Sections 2.1. As enthalpy nearly perfectly correlates with entropy,[26] we neglected the latter contribution.

2.1 | PF and CS energies

When either of the reagents is uncharged (as are $^3O_2$ and $CH_3^{\bullet}$), there is minimal electrostatic (E) interaction between reagents. Charges, however, can be induced: upon addition δ electron density shifts between D and A causing charge transfer (CT) to contribute to the reaction's overall ΔG (Equation 7). Calculation of electrostatic (E) forces (black integrals in Figure 2) as function of distance (Equations 2 and 4) is cumbersome.

Instead, free energy differences between the configurations are more easily defined (red in Figures 1 and 2). Thus, we consider the CS intermediate Φ_{CS} ($A^{\bullet -}D^{+}$) and use a thermodynamic cycle (Figure 2). Instead of calculating ΔG_{E} directly, Figure 2 provides a workaround (red arrows). We thereby calculate ΔG_{PF} from Equation 8 from ΔG_{ET} and ΔG_{CS}:

$$\Delta G_{\text{PF}} \approx n\Delta G_{\text{FO}} + \delta\Delta G_{\text{E}} = \Delta G_{\text{ET}} - \Delta G_{\text{CS}} \quad (8)$$

We calculated $\Delta(\Delta G_{\text{PF}})$ and $\Delta(\Delta G_{\text{CS}})$ values via the relative energies of FOs of the different electronic

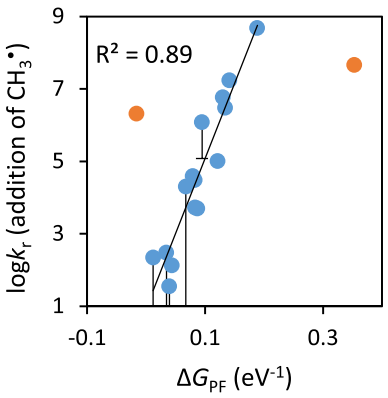

FIGURE 3 Methyl radical ($CH_3^{\bullet}$) aqueous-phase addition rate constants (y) versus free energy of product formation (PF). The x-axis is $\Delta G_{\text{PF}} = \Delta G_{\text{ET}} + \Delta G_{\text{CS}}$ (Equation 8). Orange circles represent carbon monoxide (left, may exhibit tunnelling[28]) and benzoquinone (right) (Section 4.1). E_{SOMO} of $CH_3^{\bullet}$ taken as −3.8 eV, with the SOMO as the donating orbital. The corresponding thermodynamic cycle and equations in the SI

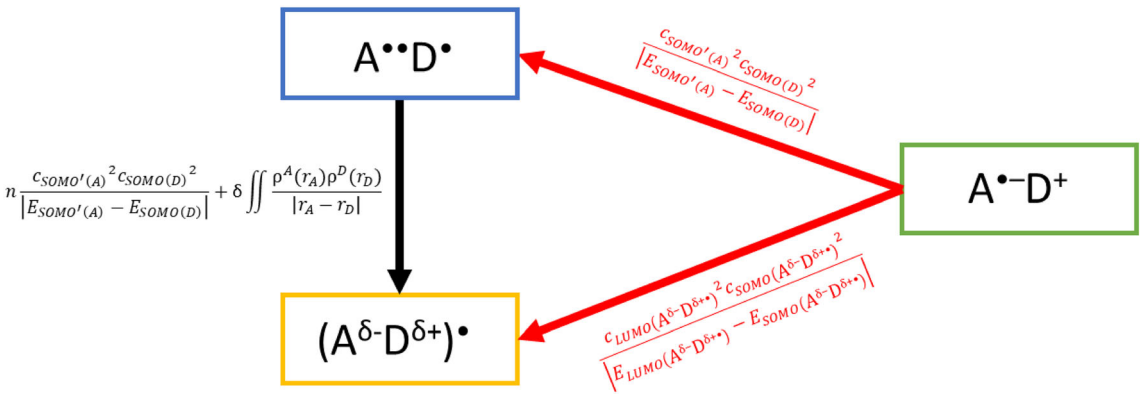

FIGURE 2 Thermodynamic cycle of radical donor (D•) and triplet acceptor (A••) reactants (blue), going via an intermediate $A^{\bullet -}D^{+}$ charge-separated (CS) excited state adduct (green) to the charge-transferred (CT) products $A^{\delta-}D^{\delta+\bullet}$ (yellow). Red arrows denote facile calculation of product formation energies ΔG_{PF} (Equation 8) from FOs. Cycles for $^3O_2$, $CO_3^{\bullet}$ and $CH_3^{\bullet}$ in the SI. FO theory rationalizes reactivity based on electron cloud overlap between donors D and acceptors A; relate to the relative energy of the product as compared with reagents[27]

configurations (Figure 2). We used experimental data for (addition) reactions involving 'soft' radicals to underpin the relevance of Equation 8: When the contribution from mixing M the CS state (in)to the TS is not significant (Equations 3 and 4) and minimal (solvent) charge stabilization, for example, for forming covalent carbon–carbon (C–C) bonds with $CH_3^{\bullet}$, the relevance of ΔG_{PF} is directly visible in patterns for k (Figure 3).

2.1.1 | Attributing donor/acceptor FOs

We selected the 'correct' roles of (intra)molecular donor and acceptor (A/D or D/A) (Figure 2) via their most favourable interaction, based orbital energies. For organic radicals (SOMO/LUMO) and triplet $^3O_2$ (SOMO′):

$$\frac{\Delta G\{A^{\bullet\bullet}D^{\bullet},A^{\bullet}D^{\bullet\bullet}\}}{p\times n}=\max\left\{\frac{1}{|E_{LUMO}-E_{SOMO}{}'|},\frac{1}{|E_{SOMO}{}'-E_{SOMO}|}\right\} \quad (9)$$

wherein n is the number of electrons transferred (here, 1) and p is an empirical (fitting) constant accounting for differences in units and reference data used to parametrize the semi-empirical quantum-chemical calculation.[29,30] When all molecules react (e.g., with $^3O_2$) via the same D/A roles, the argument in Equation 9 selects identical SOMO/HOMO/LUMO configurations for all pairs; equations are uniform. We calculated orbital energies (Equation 9) for ground-state reactants: $\Psi_{reactants}(t_{PF},r_{PF})=\Psi_{(AD)}$) and reaction products ($\Psi_{products}(t_{PF},r_{PF})=\Psi_{(A^{\delta-}D^{\delta+\bullet})}$), see Equation 2, and based on Equation 9 selected the relevant D/A.

As a brief example in line with Figures 1 and 2, Equation 9 represents SOMO′ as $A^{\bullet\bullet}$ and SOMO as $D^{\bullet}$, though the reactants can also behave as SOMO ($D^{\bullet\bullet}$) and LUMO ($A^{\bullet}$), respectively (depending on the argument in Equation 9). We calculated

$$\Delta G_{CS}\approx p\times n\left(+\frac{1}{|E_{LUMO}(A^{\delta-}D^{\delta+\bullet})-E_{SOMO}(A^{\delta-}D^{\delta+\bullet})|}\right) \quad (10)$$

which represents intramolecular excitation of the CT product $A^{\delta-}D^{\delta+\bullet}$ to the CS state. Coulombic attraction between the resulting D^+, A^- and solvent lowers TS barriers (Φ_M, Equations 2 and 4). We then obtained ΔG_{PF} via

$$\Delta G_{PF}\approx\Delta G_{ET}-\Delta G_{CS}=p\times n\left(+\frac{1}{|E_{SOMO}{}'(A)-E_{SOMO}(D)|}-\frac{1}{|E_{LUMO}(A^{\delta-}D^{\delta+\bullet})-E_{SOMO}(A^{\delta-}D^{\delta+\bullet})|}\right) \quad (11)$$

wherein $1/|E'-E|$ are the FO interaction terms (Section 2.3). The first FO interaction term in Equation 11 represents 'long-distance' (outer-sphere) electron transfer between A–D, an 'energy penalty' for moving reactants to the CS state (Figure 1).

2.2 | Hydration energies

A solvent can influence product distribution and kinetics, evidence that polarization induces electrostatic interaction with the solvent[19,31,32] (Equation 7). Figure 4 illustrates the calculation of hydration energies ΔG_{hydr} to extend the reaction diagram (Figure 1) for solvation, in equations:

$$\Delta G_{hydr,PF}=-\Delta G_{hydr}(A^{\delta-}D^{\delta+\bullet})+\Delta G_{hydr}(AD) \quad (12\text{-}1)$$

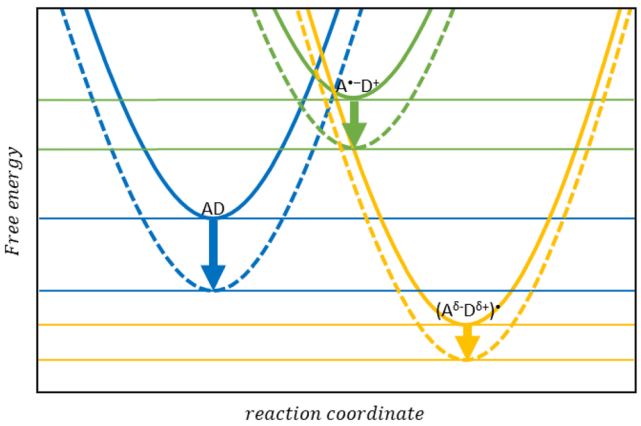

FIGURE 4 Reaction diagram and hydration energies of donor (D) and acceptor (A) reactants, going, for example, via an intermediate $A^{\bullet-}D^+$ charge transfer to products $A^{\delta-}D^{\delta+\bullet}$. For vizualization, arrow sizes (from solid unhydrated to dashed hydrated) are exaggerated. Arrow sizes denote the variability in hydration between different reactants

$$\Delta G_{\mathrm{hydr,CS}} = -\Delta G_{\mathrm{hydr}}(\mathrm{A}^{\bullet -}\mathrm{D}^{+}) + \Delta G_{\mathrm{hydr}}(\mathrm{AD}) \qquad (12\text{-}2)$$

wherein ΔG_{hydr} are hydration correction terms, the differences in hydration energies between reactants (blue) and products (yellow), and CS intermediates (green), respectively. Applying Equation (12) to include hydration, Equation 8 becomes:

$$\Delta G_{\mathrm{PF}} = \Delta G_{\mathrm{ET}} - \Delta G_{\mathrm{CS}} + \Delta G_{\mathrm{hydr}}(\mathrm{AD}) - \Delta G_{\mathrm{hydr}}\left(\mathrm{A}^{\delta-}\mathrm{D}^{\delta+\bullet}\right) \qquad (13)$$

Hydrations of CS intermediates (adducts, green) are more similar than hydrations of heterogeneously functionalized (e.g., charged/uncharged) reactants (blue). Therefore, the variation in hydration for reactants on $\Delta G^{\ddagger}$ (contribution thereon) exceeds that of CS intermediates or products (Figure 4). As also the contribution from (A) to $\Delta G_{\mathrm{hydr}}(\mathrm{AD})$ is identical for all its reactant pairs, we simplify Equation 13 by

$$\Delta_{12}\left(\Delta G_{\mathrm{hydr}}(\mathrm{AD}) - \Delta G_{\mathrm{hydr}}\left(\mathrm{A}^{\delta-}\mathrm{D}^{\delta+\bullet}\right)\right) \approx \Delta_{12}\Delta G_{\mathrm{hydr}}(\mathrm{D}) \qquad (14)$$

in which we took $\Delta G_{\mathrm{hydr}}(\mathrm{D})$ as the difference in heat of formation (HoF) of the reactant molecule in water and a vacuum (Figure 5). We validated its relevance via $\Delta G^{\ddagger}_{\mathrm{hydr}}$, the experimental perturbation due to hydration energies

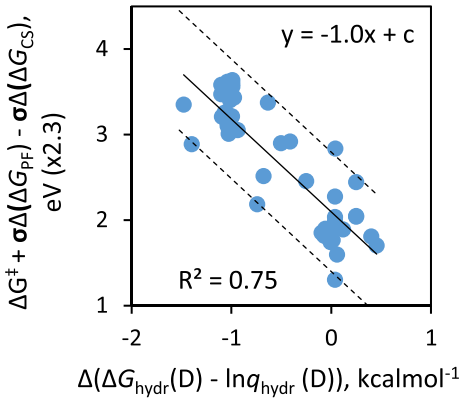

FIGURE 5 Parametrization of hydration. *y*-axis is the residual activation energy (reaction with A = $CO_3^{\bullet -}$) after considering (i.e., correcting for) PF and CS (Equation 5), in eV. *x*-axis is hydration energy (in kcal mol^{-1}) of electron donor (D), minus the natural logarithm of the frequency factor $\ln q_{\mathrm{hydr}}$ ($\sim\ln SASA(\mathrm{D})$) (in Å). Dashed lines are factor 5 deviations ($\approx 2\sigma$) from fit (solid line). The regression reflects the relevant charges in reactants to be homogeneously distributed

(*y*-axis in Figure 5): the difference between independent experimental $\Delta G^{\ddagger}$ ($CO_3^{\bullet -}$) and $\Delta G^{\ddagger}$ that would be expected based on $\sigma\Delta$ (ΔG_{PF}), $\sigma\Delta$ (ΔG_{CS}) (Section 2.1) and frequency factors (Section 2.3) (Figure 5).

2.3 | Frequency factors *q*

For (inner-sphere) addition, solvent (water) at the (~1) reaction centre needs to reorientate to allow reaction. The 'frequency' by which H_2O blocks reactive sites (D/A FOs) depends on the structure and size of the hydration complex. Though $\Delta G_{\mathrm{hydr}}(\mathrm{D})$ (Equation 14) encompasses the full molecule, only part of it reacts. We therefore defined and applied a 'hydration frequency':

$$\ln\left(q_{\mathrm{hydr}}\right) \equiv \sigma_{\mathrm{hydr}}\Delta\left(\Delta G_{\mathrm{hydr}}(\mathrm{D})\right) - \Delta\left(\Delta G^{\ddagger}_{\mathrm{hydr}}\right) \approx \ln\left(\frac{SASA_{\mathrm{FO}}}{SASA_{\mathrm{D}}}\right) \qquad (15)$$

as the reciprocal of the FO's area over the total area (SASA) of D able to interact with water ($q_{\mathrm{hydr}} = SASA_{\mathrm{FO}}/SASA_{\mathrm{D}}$). We validated its relevance by calculating 'experimental' q_{hydr} (Equation 15, Figure 5).

Looking past solvent rearrangement, the dimensions (r and t) of configurations Ψ and Φ need to match (for both PF and M to take place) with sufficient frequency for a reaction. Electrons delocalize to neighbouring atoms as a function of orbital coefficients, characterizing 'electronic coupling'[33] (F_c, Equation 5). The frequency (pre-exponential) q (Equations 1, 6 and 15) (cor)relates to density coefficients.[19]

$$q = f\left\{c_{\mathrm{LUMO}}(\mathrm{A})^2 c_{\mathrm{SOMO}}(\mathrm{D})^2\ ,\ c_{\mathrm{LUMO}}\left(\mathrm{A}^{\delta-}\mathrm{D}^{\delta+\bullet}\right)^2 c_{\mathrm{SOMO}}\left(\mathrm{A}^{\delta-}\mathrm{D}^{\delta+\bullet}\right)^2\right\} \propto F_c \qquad (16)$$

We deal with similarly sized small organic molecules (those assessed for [environmental] risk,[34–36] SI3) in which electrons hybridize in similar geometries and a uniform reaction mechanism (addition). Therefore, there is limited variation in orbital shape (electron space) and overlap/resonance.[11] Hence, we take F_c (Equation 5) and overlap terms $c_{\mathrm{R2}}{}^2/c_{\mathrm{R1}}{}^2$ as constant factors ($\Delta_{12}F_c = 0$; $\Delta_{12}c^2 = 0$) (Section 1.1). By extension, q in Equation (1) is constant[19] (Figure 6). This was with exception of purine/nucleoside radicals[37]: for adenosine/guanosine (R1), we applied the maximal FO density of the SOMO (−6.0 eV) on a carbon: $\log\left(c^2_{\mathrm{R1}}/c^2_{\mathrm{R2}}\right) = -2$.

Shapes of potential curves (r) affect importance of $\Delta(\Delta G_{\mathrm{CS}})$ relative to $\Delta(\Delta G_{\mathrm{PF}})$ (endo/exothermicity, Figure 1), via σ values (Equation 5).[19,38,39] From literature,[19,40,41] we obtained a constant value of $10^{2.3}$ M^{-1} s^{-1} eV^{-1} for σ_{PF}. Via a radical channel/

pathway, electrophilic aromatic substitution for various reagents adheres to CS: Transition energies ($-\Delta h\nu/2.3RT$) correlate with $\log(k_{R1}/k_{R2})$ with a slope of ~1; thus, $\sigma_{CS} = 10^{2.3}$ M^{-1} s^{-1} eV^{-1}.[20] We verified the constant σ_{CS} value by calculating it from $\Delta(\Delta G^{\ddagger})$ data for uncharged reactants by solving σ_{CS} $\left[\Delta(\Delta G^{\ddagger}) - \sigma_{PF}\Delta(\Delta G_{PF})\right]/\Delta(\Delta G_{CS})$ for least squares. We validated our treatment of σ and q with independent data (on $CO_3^{\bullet-}$) (Figures 5 and 7):

3 | RESULTS

We applied a universal LFER (Equations 3 and 5) built on a thermodynamic cycle involving a CS intermediate (Figure 2). We validated our calculations of $\Delta(\Delta G_{PF})$ values (Equation 8) by screening their relevance for addition-type reactions involving $CH_3^{\bullet}$. The correlation of ~90% (Figure 3) entails the outliers carbon monoxide and benzoquinone (reacting under pH of 1–2 and 5.4, respectively) denoting the limits of applicability of Equation 8. 'Soft radicals' (like $CH_3^{\bullet}$) form covalent bonds, with the net transfer of not one, but two electrons into a new orbital.[42] If two electrons combine into a new covalent bond, radical–radical reactions ought to proceed via $k_r \sim 10^{n\cdot 2.3}$ M^{-1} s^{-1} eV^{-1}, with $n = 2$. This $k_r \sim 10^{4.6}$ M^{-1} s^{-1} eV^{-1} relationship is the lower limit of $^3O_2$ addition rate constants: >95% of k_r values are higher than expected on the basis of $\sigma_{PF}\Delta G_{PF}$ (i.e., $k_r \sim 10^{4.6}$ M^{-1} s^{-1} eV^{-1}) (Figure S1). In other words, $\sigma_{CS}\Delta G_{CS}$ (green parabola in Figure 1) for $^3O_2$ cannot be ignored (>0). The same is true for $CO_3^{\bullet-}$. Table 1 depicts the inverse involvement of CS (in green), relative to PF (yellow).

We subsequently calculated ΔG_{CS} for different transitions (CS) involving $^3O_2$ and $CO_3^{\bullet-}$ (Equations 8 and 9) and used experimental k_R values to parametrize an LFER and extract information on σ_{CT}. This quantified the influence of mixing of the CS state on $\Delta G^{\ddagger}$ values, λ_M. The results show that for the addition of $^3O_2$, depending on fitting ($E_{SOMO}(^3O_2) = -4.6$ to -4.2 eV), the value for $(\lambda_M/F_c)\cdot\sigma_{CS} = 10^{2.3-2.6}$ M^{-1} s^{-1} eV^{-1} (Figure 8). This result did not differ from σ_{CS} obtained by Fukuzumi and Kochi.[20] Because $F_c \lessapprox 1$ (Sections 2.1.1 and 2.3), we can infer that the value for λ_M for addition reactions with $^3O_2$ is $\lambda_M = F_c\cdot(\sigma_{CS}/\sigma_{CS,ref}) = F_c\cdot(10^{2.3-2.6}/10^{2.3}) = 10^{0-0.3}$. Hence, λ_M is approximately a constant factor, near unity. The relative sizes of $\Delta(\Delta G_{CS})$ and $\Delta(\Delta G_{PF})$ values for $CH_3^{\bullet}$ addition reactions did not allow calculation of (experimental) λ_M for $CH_3^{\bullet}$.

Intramolecular excitations of neutral ground-state molecules produce 'charge-polarized' states (species) with increased polarity[43] (Table 1 and SI). Including hydration of neutral molecules for ΔG calculations

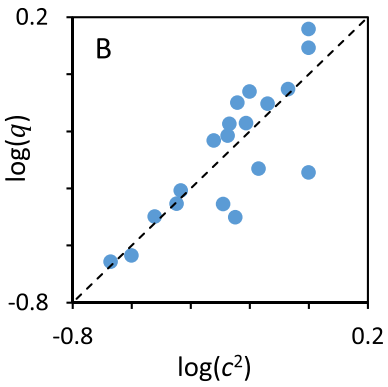

FIGURE 6 The statistical factor q (on the y-axes) correlates with squared atomic orbital coefficient (here, of HOMO). The dashed line denotes theoretical relationships for symmetry. Reproduced from Nolte et al

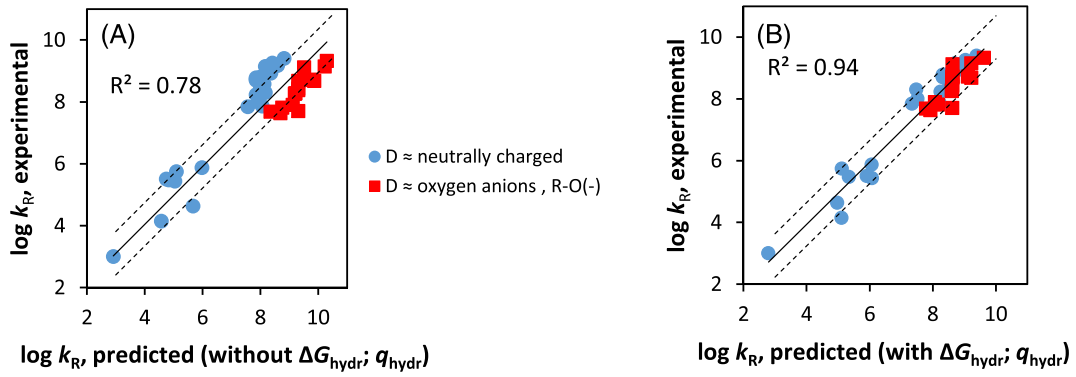

FIGURE 7 Experimental (y) versus predicted (x) rate constants (k_R), reactions between organic molecules (D) and the carbonate radical anion $CO_3^{\bullet-}$ predicted based on fitting to q_{hydr} and substituent constants σ for PF ($10^{2.0\pm0.2}$ M^{-1} s^{-1} eV^{-1}, 1 SD), CS and hydration ($10^{1.8\pm0.3}$ M^{-1} s^{-1} eV^{-1}, 1 SD). Without (A) and with (B) inclusion of hydration (Equations 14 and 15). Dashed lines show a factor 5 deviation (≈2 SD) from the fit (solid line). Variance in q_{hydr} is larger than contributions to q by orbital overlaps, substantiating it taken as constant

TABLE 1 Relative covalency (softness) of reaction with $^3O_2$ (%) as analogous to literature[22]

Hydrogen	100	*N*6,*N*6-Dimethyladenosine (8-OH)	0
Methanol	74	Adenosine	5
Ethyl	73	Guanosine	6
Cyclopentyl	72	Iodine atom	8
Methoxymethane	72	Deoxycytidine	8
Neopentane	72	Nitrobenzene	9
1-Methylpropyl	71	Flavone-8-methyl	9
2-Hydroxyethyl	70	3,5-Dihydroxyphenoxyl	12
Methyldiol	70	Phenoxyl radical	12
Ethylene glycol	68	Nitroxyl (HNO)	13
1-Hydroxypropyl	67	4-Cyanophenyl	16
2-Methoxy-2-methylbutane	67	*N*6,*N*6-Dimethyladenosine (5-OH)	18
Methyl	66	4-Chloroanisole	18
Hydrazine (singlet state, non-radical)	64	Benzoic acid (m)	18
2-Butanol	63	Cyanobenzene (m)	18
Isopropanol	63	Ethyl benzoate (m)	20
Methyl acetate	63	*N*6,*N*6-Dimethyladenosine (4-OH)	20
2-Propan-2-yloxypropane	63	Cytosine (5-OH)	20
Tertbutanol	62	Chlorobenzene (o)	21
2-Methoxy-2-methylpropane	62	Pentachloroethyl	23
Dimethylaminomethyl	59	Naphthalene	24
Hydrazine radical	59	Fluorobenzene (p)	25
2-Methoxy-2-methylpropane	58	2-Pyridyl radical	25
Sarcosine anhydride	54	Thymidine (6-OH)	26
2-Hydroxyethenyl	47	1,2-Dichloro-1,2,2-trifluoroethyl	26
Chloromethyl	46	Dichloro(cyano)methyl	26
2,2,2-Trifluoro-1-(difluoromethoxy)ethyl	45	Benzene	28
Amino radical	41	1,3-Dimethyluracil (6-OH)	28
Alanine anhydride	40	Methoxybenzene (o)	30
1-Chloro-2,2-difluoro-2-methoxyethyl	40	Cytidine (5-OH)	30
Uracil (5-OH)	40	4-Methoxyphenyl	31
Thymine (5-OH)	39	Phenyl radical	31
Sarcosine anhydride	39	Trichloromethyl radical	33
1-Chloro-2,2,2-trifluoroethyl	39	Toluene (o)	35
Uridine (5-OH)	38	Chloral	35
Glycine anhydride	38	Phenol (o)	37
Thymidine (5-OH)	38	1,2,2-Trifluoro-2-(difluoromethoxy)ethyl	38

Note: By our definition, the relative covalency is $\Delta G_{PF}/(\Delta G_{PF} + \Delta G_{CS})$. The colours indicate the strength of PF and CS, corresponding to colours in Figures 1 and 2. The relative covalency is inversely related to λ_M.

(Equations 13–15) did not visibly contribute to a better fit for $^3O_2$. For a set of uncharged molecules reacting with $^3O_2$, Equations 13–15 result to give a maximum average value for $\sigma_{PF}\Delta\left(\Delta G_{hydr,PF}\right) = 1.4$ kJ mol^{-1}[19] (SI), negligible as compared with experimental $\Delta(\Delta G^{\ddagger})$. For charged species, however, the contribution however is not negligible. For charged and polar molecules reacting with $CO_3^{\bullet-}$, Equations 13 and 14 improved our

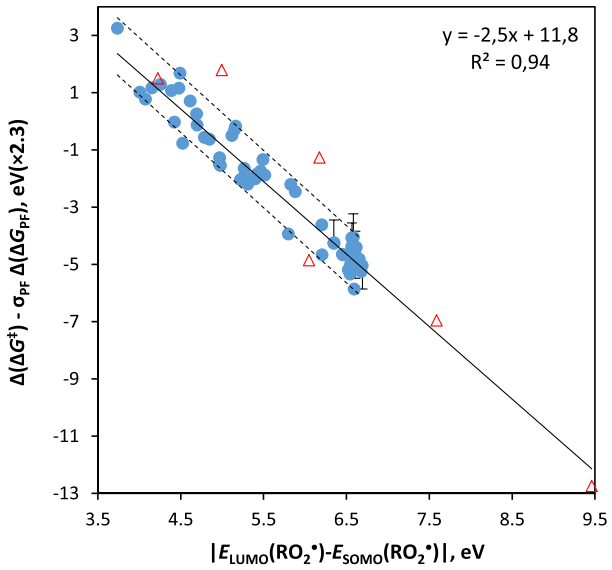

FIGURE 8 Mixing (y) versus the energy gap intramolecular excitation energy of the RO_2 adduct ΔG_{CS} (x). y values are given as follows: $\log(k_R) + (2.3 \cdot (|-4.2 - E_{SOMO}(R^{\bullet})| - |E_{LUMO}(RO_2^{\bullet}) - E_{SOMO}(RO_2^{\bullet})|)$. The slope of the regression gave (λ_M/F_c). Calculation of the SOMO of $^3O_2$ gave $E_{SOMO} = -4.6$ eV, fitting set it to −4.2 eV. Blue circles are small organics; red open triangles are inorganics

prediction of k_R from $R^2 = 0.78$ to $R^2 = 0.94$ (Figure 7). We found several outliers for the relationships. For the most part, we had anticipated these (i.e., data curation in SI3). Outliers represent inorganic molecules (Figure 8), varying solvent use (Figure 11) and experimental quirks (see Sections 4.1–4.4).

4 | DISCUSSION

Our results show that addition-type reactions with $^3O_2$ and $CO_3^{\bullet -}$ involve significant CS and CT, in contrast to $CH_3^{\bullet}$. CS and delocalization during the TS perturb simple ('non-universal') LFERs. Addition universally proceeds according to $(\lambda_M/F_c) \cdot \sigma_{CT}$, which is equal to $(\Delta G^{\ddagger} + \sigma_{PF} \cdot \Delta G_{PF})/\Delta G_{CT}$, calculated to be ~2.3 M^{-1} s^{-1} eV^{-1}. The F_c (coupling) term, by approximation, is a product function entailing orbital density coefficients for intramolecular and intermolecular FO overlap. Within non-complex (small) molecules, this term is indeed constant. Seeing as $\sigma_{CT} = 2.3$ M^{-1} s^{-1} eV^{-1},[20] for example, the contribution by $^3O_2$ to λ_M is approximately a constant factor near unity. The combined results, when compared with previous study, illustrate benefits of preferentially using our universal LFER method over existing methods (see Section 4.5).

Variation in λ_M can be fully explained by variability between experimentation, with limited involvement of c^2 or F_c (see Section 4.4; SI). Consequently, by approximation, λ_M is a constant factor for a given radical: For small organic molecules, there is no visible variation in λ_M. This does not necessarily agree with 'ab initio' simulations. Herein, the λ_M term (Equation 2) may therefore be merely a parameter to fit the 'ab initio' simulations to observed data. This is scientifically not very satisfactory. We cannot see a reason why λ_M for $^3O_2$ should vary between small organic reagents; if a mechanistic explanation for variation is absent, it should be treated as a constant a priori.[44] This reflects the intimate connection between CS (polarization) and PF (polar) energies.[27] LFER relies on accurate and precise determination of these ΔG values, discussed in Sections 4.1–4.3.

We applied and tested algebra combining both 'hard' (ionic) and 'soft' (covalent) interactions to estimate $\Delta G^{\ddagger}$. Our combination of both limits exposed a universal linear free energy relationship, exemplified for $^3O_2$, $CO_3^{\bullet -}$ and organic molecules. The extent of the mixing λ_M (differing between the added reagents) handily characterizes the extent of CS interactions by distinguishing between hard from soft mechanisms (Figure 9). Electrophilic reagents (e.g., Br_2, Cl_2 and RF_3) produce highly relevant CT species[20,42,45]: A high value for λ_M denotes a high correlation between $\Delta(\Delta G_{CS})$ and $\Delta(\Delta G^{\ddagger})$ as shown by $\Delta(\Delta G^{\ddagger})$ $(\lambda_M/F_c)\sigma_{CS}\Delta(\Delta G_{CS}) + \sigma_{PF}\Delta(\Delta G_{PF})$.[20] Then, the contribution from $\sigma_{PF}\Delta(\Delta G_{PF})$ might be neglected (Figure 9A). This however breaks down for softer reagents/mechanisms (Figure 9B).

4.1 | Product formation ΔG_{PF}

One-electron ($n = 1$) oxidation involves relationships with reaction exothermicity $k_R/\Delta G_R \propto 10^{n \cdot 2.3 \pm 0.1}$ M^{-1} s^{-1} eV^{-1}.[19,40] When FOs interact, the relative energy of $A^{\bullet -}$ and D^{+} (e.g., $O_2^{\bullet -}$ and R^{+}) with respect to the ground-state energies of A and D, ΔG ($O_2^{\bullet -}$, R^{+}), is proportional to $|E_{SOMO}(R) - E_{SOMO}(^3O_2)|$. The data we applied not adhered to this, because they do not represent one-electron oxidation (or recombination, $n = 2$). Instead, for addition, a non-integer number of electrons moves between D and A and additional (coulombic) interactions can exist (Figure 2).

Singlet (ground-state) organic molecules have all electrons paired. $^3O_2$ cannot receive a pair of electrons because this requires spin inversion, prohibited by the spin conservation rule (Hund's rule). The few singlet state chemicals included here (e.g., hydrazine as the bottom-right red triangle in Figure 8) follow the expected low reactivity. The paramagnetic biradical $^3O_2$ tends to

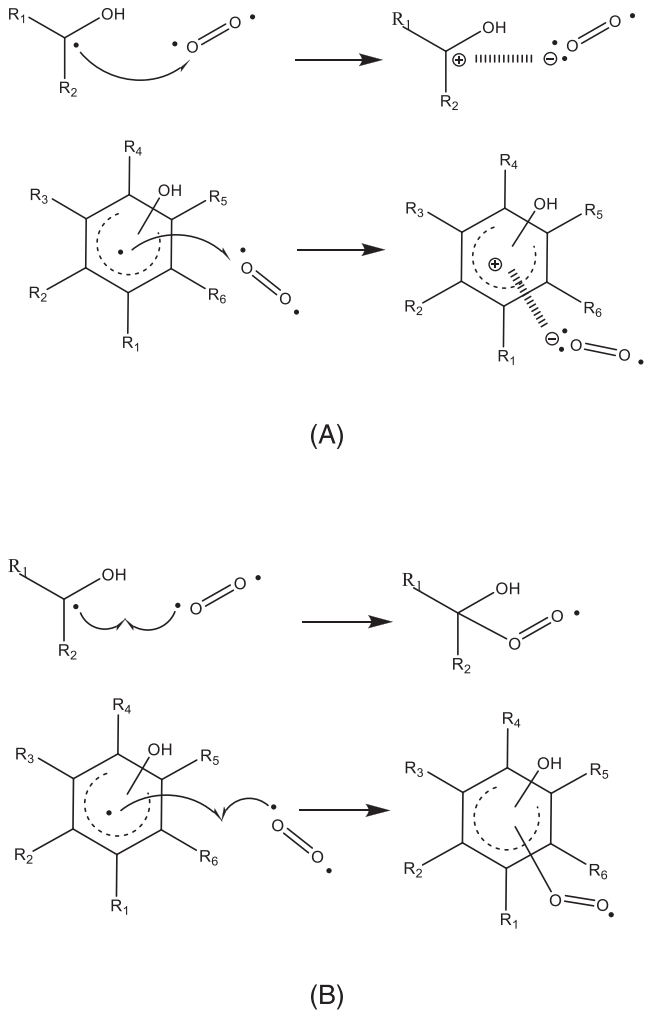

FIGURE 9 (A) Illustration of binding of $^3O_2$ were it a 'hard–hard', or ionic mechanism. Note the prominent charge transfer (CT) and separation (CS), that is, high λ_M. (B) Illustration of binding of $^3O_2$ were it a 'soft–soft', or covalent mechanism. Note the lack of charge transfer (CT) and separation (CS), that is, low λ_M

receive electrons by one-electron steps, reacting rapidly with, for example, radicals. Carbon-centred radicals often add $^3O_2$ at (or near) diffusion-limited rates $k_R \sim 10^9$ M^{-1} s^{-1} being essentially barrierless,[46] observed for numerous compounds, for example, glyoxal[47] (Table 1) (yellow).

In case of aromaticity and when electron density resides on heteroatoms, smaller k_R have been observed, with $k_{(R^\bullet + O2)} \approx 5{\cdot}10^6$ to $5{\cdot}10^8$ M^{-1} s^{-1}.[47] Adenyl and guanyl radicals have their unpaired electron on O and N (i.e., non-carbon centred), hence low reactivity.[37] According to Klopman and Salem,[25,48,49] atomic orbital coefficients (c) need be included in the calculation of ΔG. Values for c also characterize the pre-exponential frequency factor $(kT/h)\cdot q$ (Equation 1).[19] When 'correcting' for c or q ($\sim$0.006), the data were within those expected based on LFER (Figure 8).

Electrophilic attack (by $^3O_2$ and $CO_3^{\bullet-}$) prefers the most negative charge on a molecule. An electron-withdrawing group reduces the partial negative charge on ortho and para positions of an aromatic compound. Thereby, electrophilic addition is inhibited for those positions, but expected to occur mainly on the meta position.[50] With insufficient such selectivity, addition of $OH^\bullet$ produces a mixture of hydroxycyclohexadienyl radicals. For a mix of different radicals with site-specific electron densities in different concentrations, it becomes uncertain which species has the highest reactivity, that is, which factors drive the observed kinetics (green stars in Figure 10).

4.2 | Mixing ΔG_{CS}

For $CH_3^\bullet$ addition, reaction exothermicity dominates reactivity.[52] π-electron-accepting substituents (e.g., to alkenes) enhance reactivity via ΔG_{PF} for PF. For $CH_3^\bullet$, polar contributions to the TSs are of minor consequence to $\Delta G^\ddagger$,[53] but PF can include polar effects[54]; PF can explain $\sim$90% of its reactivity (Figure 3). Figures 3 and 7/8 illustrate the difference between $CH_3^\bullet$ and $CO_3^{\bullet-}/^3O_2$. For $^3O_2$ and $CO_3^{\bullet-}$, in contrast, similar model performance is only obtained by considering both PF and CS in the TS (Figures 7 and 8). Illustratively, ΔG_{PF} (i.e., E_{SOMO} of $R^\bullet$) values between MAHs and PAHs generally differ. Toluene-OH, however, ($4.5{\cdot}10^8$ M^{-1} s^{-1}) does not add $^3O_2$ significantly faster than does $C_{10}H_8(OH)$ or $CH_3C_{10}H_7(OH)$ ($5(\pm1){\cdot}10^8$ and $4.2(\pm1){\cdot}10^8$).[21] We infer, then, that ΔG_{PF} does not solely determine reactivity, but CS and CT must be involved. If everything else is constant, values for λ_M differ between radicals: for example, $\lambda_M(CH_3^\bullet) < \lambda_M(^3O_2)$.

Intermolecular and intramolecular CS configurations are excited state configurations, generated by ET between donor D and acceptor A (Figure 2). The change in $\Delta G^\ddagger$ is proportional to the energy gain from the interaction between D^+ and A^-, $\sim 10^{2.3}$ or $10^{4.6}$ M^{-1} s^{-1} eV^{-1} depending on how many electrons the interaction involves (Figure 2). An example is the reaction between the thymine radical anion ($T^{\bullet-}$) and $^3O_2$, which possibly involves a superoxide ($O_2^{\bullet-}$) intermediate ($T–O_2^{\bullet-}$).[55] Reaction between $^3O_2$ and metal oxide surfaces produces $O_2^{\bullet-}$ as a CT species, attaching to the surface via electrostatic or covalent bonding.[56] These intermediates can be long lived, so that the involvement of charge separation can even be directly observed.

Some hydroxycyclohexadienyl radicals with electron-withdrawing groups (e.g., N≡C, NO_2) are less reactive as

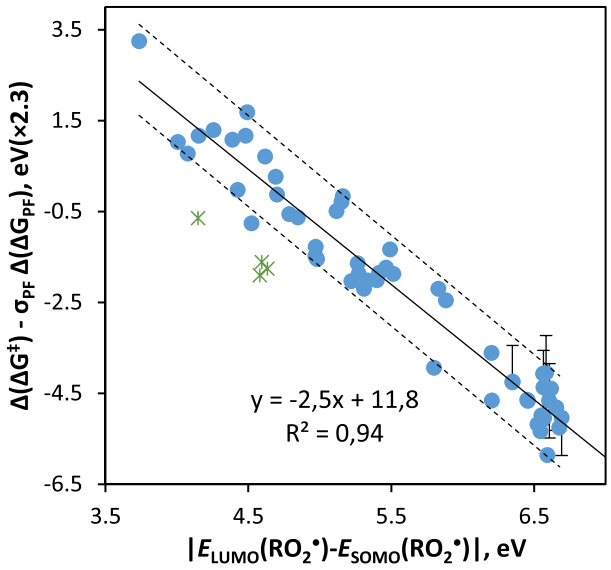

FIGURE 10 Mixing and charge-separation (CS) energy (y) versus the energy gap of intramolecular excitation of the RO_2 adduct (x). y values are $\sigma_{CS}{\cdot}\Delta G_{CS}$ calculated as $\log(k_R) + (2.3{\cdot}(|{-}4.2 - E_{SOMO}(R^{\bullet})| - |E_{LUMO}(RO_2^{\bullet}) - E_{SOMO}(RO_2^{\bullet})|)$. Blue circles are small organics; green stars are hydroxycyclohexadienyl radicals with (strong) electron-withdrawing substituents[51]

predicted (Figure 10). Rather than single compounds, the underlying k_R data represent mixtures of reagents, facilitating errors when the calculus does not reflect a combination of multiple reactions (Section 4.1).[51] We cannot substantiate this explanation because an additional explanation is low orbital overlap (F_c in Equation 3) as involved with CT. F_c for, for example, a nitrated CS complex is probably small: The LUMO of $O_2^{\delta-}R^{\delta+}$ resides on carbons (e.g., ${c_{C5}}^2 = 0.4$) and the nitro group (${c_{nitro}}^2 = 0.3$), but no relevant SOMO electron density resides here (${c_{C5}}^2 = {c_{nitro}}^2 = 0.0$). Rather, the SOMO resides on the dioxygen (${c_{O10}}^2 = {c_{O11}}^2 = 0.5$). If orbitals are not part of the same functional group (e.g., in $O_2^{\delta-}R^{\delta+}$), electronic excitation in $O_2^{\delta-}R^{\delta+}$ to form the intramolecular CS complex $O_2^{-}R^{+}$ (green in Figures 1 and 2) is problematic. λ_M may characterize whether an early or late TS is involved,[52] in this case, late (simplifying q in Equation 16).

4.3 | Hydration ΔG_{hydr}

In this study, we anticipated hydration to affect the chemical potential of either more of reagents or intermediates (Section 2.2). Gaseous density functional theory (DFT) calculations show that both hydrogen abstraction (HA) by O_2 and addition of O_2 to the π-delocalized system are viable,[57–59] with hydration affecting the reaction pathway.[60] Aromatic cations are relatively inert in H_2O[1] attributable to solvent effects and outer-sphere mechanisms.[40] When aqueous reactions involve movement of more than one electron, k_R decreases by more than a factor 10 when the reaction centre is near charge-carrying groups.[19,38,61] If no clear (integer) number of electrons transfers, it can be unclear how hydration affects addition mechanisms.

Between neutral reagents, the involvement of hydration on the addition kinetics seems limited. This is evidenced by the observation that inclusion of ΔG_{hydr} (Equations 13 and 14) did not visibly improve the correlations for $^3O_2$: $\Delta(\Delta G_{hydr})$ values are small as compared with $\Delta(\Delta G_{PF})$ (Section 2.2). For hydroxycyclohexadienyl radicals, reactivity in the gas and aqueous phases follows the same trends.[62] The effective polarity depends also on the polarizability, that is, CT. Adducts are more similar to each other in terms of polarity, as compared with the starting reagents: We anticipated larger $\Delta(\Delta G_{hydr})$ for going from AD to $A^-D^{+\bullet}$, as compared with going from $A^{\delta-}D^{\delta+\bullet}$ to $A^-D^{+\bullet}$ (Section 2.2). The low relevance of ΔG_{hydr} may therefore be due ΔG_{hydr} correlating with ΔG_{CS} as suggested before.[54,63] By describing $\Delta(\Delta G_{CS})$ via FOs (Equations 8 and 10), potential errors resulting from the ΔG_{hydr} term are minimal.

From results on reactions between charged chemicals and $CO_3^{\bullet-}$, we see that hydration influences $\sigma^{-1}\Delta G^{\ddagger}$ by ~100 kJ mol^{-1} (~1 eV) (Figures 5 and 7). This is equal to 10–25 hydrogen bonds, which need to be broken in order for a reaction to occur. We can also calculate activation energies based on polarity: $\Delta(\Delta G^{\ddagger}) = \Delta(\Delta G^{\ddagger}) - z{\cdot}\mu$, wherein $z = 0.8$ kJ mol^{-1} D^{-1}[19] and μ is the dipole moment of the organic molecule. For, for example, zwitterionic compounds ($\mu = 10$–15 D), the effect on $\sigma^{-1}\Delta G^{\ddagger}$ is also ~100 kJ mol^{-1}. In contrast, a set of uncharged molecules (reacting with $^3O_2$) with dipole moments (μ) of ≤5 D entail values for $\Delta(\Delta G^{\ddagger})$ of 'only' ≤4 kJ mol^{-1}.[19] This agrees with results from Equation 8 for compounds attaining no net charges: much smaller $\sigma\Delta G_{hydr}$ than experimental variability in $\Delta G^{\ddagger}$ values, that is, negligible. Even 'ab initio' methods can incorrectly characterize polarity/hydration effects to $\Delta G^{\ddagger}$[54]; our semi-empirical approach can have similar drawbacks[40]: Erroneously correcting ΔG for hydration will introduce errors in predictions for $\Delta G^{\ddagger}$.

4.4 | Variability and uncertainty

Our error (2 SD) is a factor ~5 (in k_R, Figures 7 and 8). Predictions for one-electron oxidation using one parameter have 30%–40% error.[19] Multiplicative error

propagation shows Equation 8 to involve 42%–57% error (i.e., a factor ~2). A portion of the uncertainty lies in the k_R data used to parameterize our universal LFER. Laboratory 'k_R' values differ widely: For example, for pyruvic acid, $k_{(R^\bullet + O2)} \approx 10^6$ M^{-1} s^{-1}, 1000 times lower than an earlier value.[47] For benzene[64,65] and isopropanol,[66,67] factors 100 and 7 variability exist, respectively. A factor 2–3 variability is more common: 1.5–3.1·10^8 M^{-1} s^{-1} for $^\bullet$OH-benzene.[51,68,69] Studies exclude structurally similar compounds with a factor >2 variability, k_R for $^\bullet CH_2CH_2OH$ and $CH_3COO^\bullet CH_2$ (6.6–14·10^9 M^{-1} s^{-1}): 'too inconsistent'.[70]

Halogenated compounds react fast (orange diamonds in Figure 11) in mixed solvent (<95% H_2O).[71,72] This affirms that our modelling adheres to the aqueous phase. Apolar solvents increase the potential of polar reagents (blue, Figure 1). Polar solvent or ionic strength (i.e., higher dielectric constant) stabilizes the ground and excited states to different extents (producing solvatochromic shifts), promoting ionic TSs.[31,32,73,74] Typical measurement variability for solvent partitioning is a factor ~2,[75] indicative of variability in experimental results for kinetics using different co-solvents. Adding 10% apolar solvent (octanol) to a 'hydrophobic' compound (e.g., $K_{OW} > 10$) can influence its rate by >50% ($k/k_{obs} = 1 + (10\%/100\%)K_{OW}$[76]) by affecting the compounds hydration sphere. Therefore, the 5% solvent exclusion criterion (SI3) is not conservative. As k_R might be enhanced 10-fold (Figure 11), extrapolating predictions to other solvent (mixtures) should be done with caution.

When conditions vary, side reactions convolute kinetic measurements. Bimolecular disproportionation and dimerization occur via $\gtrsim 1{\cdot}10^8$ M^{-1} s^{-1}[68,77,78]; for a 50-μM yield, $k_{obs} \sim 5{\cdot}10^3$ s^{-1}, convoluting experimental signals for addition, more so for inert compounds. $OH^\bullet$ reacting with t-BuOH ($k = 6{\cdot}10^8$ M^{-1} s^{-1}) will, when $^3O_2$ is added, coincide with reaction between $R^\bullet$ and $^3O_2$ (1.8·10^9 M^{-1} s^{-1}).[79] Isomerization of $HRO_2^\bullet$ to $ROOH^\bullet$[80] (H-shifts[81]) influences $\Delta(\Delta G)$ representing different/varying products.* Reaction with carbon monoxide (CO) may involve proton (cation) transfer (PT)[82]; thus, CO need not adhere to LFER because PT renders ΔG_{PF} uncertain (Figure 3). CO and the monodehydroascorbate radical ('rapid reaction with O_2',[83] or <5·10^2[84]) may be sensitive to pH, solvent and (other) catalysts/contaminants. 'Anomalous' large redshifts of absorption maxima of the di-meta-methoxyl phenol radical[85] may convolute measurements for $CO_3^{\bullet -}$[86] (similar for benzonitrile, Table S3). We may calculate influences of all such factors (if 'properly' reported) on ΔG, but left unaccounted for when modelling, uncertainty increases. Variability in k_{obs} underpins the need for data curation (SI3). Most of our prediction error relates to undocumented variability.

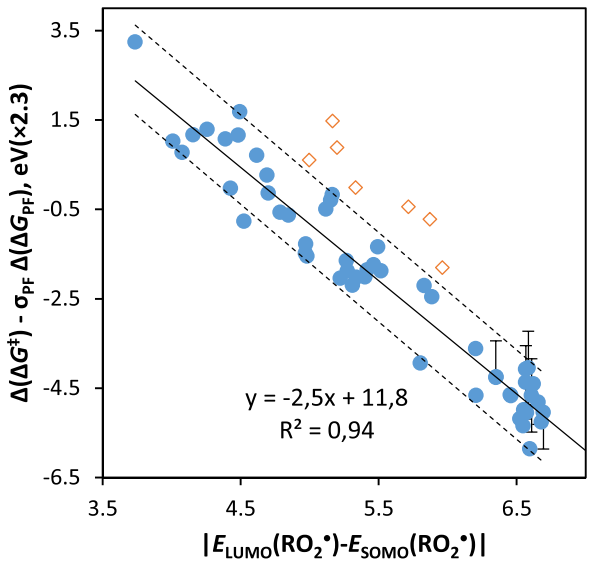

FIGURE 11 Mixing and charge-separation (CS) energy (y) versus the energy gap intramolecular excitation energy of the RO_2 adduct (x). y values are $\sigma_{CT}{\cdot}\Delta G_{CS}$ calculated as $\log(k_R) + (2.3{\cdot}(|-4.2 - E_{SOMO}(R^\bullet)| - |E_{LUMO}(RO_2^\bullet) - E_{SOMO}(RO_2^\bullet)|)$. Blue circles are small organic molecules in 100% H_2O; orange open diamonds are experiments for which the solvent was <95% H_2O. Experiments with halogenated compounds contained 3.7%–7.4% non-H_2O

4.5 | Unlocking semi-empirical advantages

We applied and tested facile, computationally inexpensive ('cheap') LFER parameters to predict k_R values for radical addition. Irrespective of the radical substrate ($^3O_2$, $CO_3^{\bullet -}$, $CH_3^\bullet$ etc.), our universal LFER demonstrates accuracy of ~94% (in terms of R^2, Figures 3, 7 and 8). Semi-empirical methods are often considered having a disadvantage of being less accurate than ab initio calculations, which 'must be done' if high accuracy or precise intermolecular comparisons are required. We find, however, that this need not necessarily be the case. Semi-empirical methods can appear equally accurate because of cancelling out of systematic errors. If known which errors are involved, appropriate calculus allows such cancelling. Our study demonstrates this for addition rate constants.

Our calculation time for 100 reactions is <1 h on a standard desktop PC, similar to recent findings[19,87,88]; 100,000+ chemicals, reagents and reactions need to be assessed.[7,8] Intensive and expensive ab initio methods or experimentation (upon which statistical models are parametrized) may take decades, hence is virtually

impossible.[9] For example, direct study of CT energies (black arrow, Figure 2) via 'ab initio methods' is cumbersome. Extrapolating results from our 'cheap' computational method shows that screening extended compound libraries among 100,000+ possible reactions takes only ~1 month, which is practical and cost-effective. This allows selecting only 'problem' and 'priority' substances that require further (experimental) study, reducing costs.

While ab initio helps to characterize adduct formation, it can underestimate radical stabilization and polar effects of substituents on addition barriers.[54] Conversely, statistical methods and complex descriptors ('black box machine learning') lack intuitiveness and improve Quantitative Structure-Property Relationships (QSPRs) by only 10% at a loss of underlying mechanistic interpretation.[89] Better understanding enables more straightforward extrapolation to other reactions, conditions, species and so forth. This prompted us to take worthwhile aspects of different methods[90] and pursue a universal LFER methodology capturing the interplay between bonding type, charge-carrying and electron-withdrawing/donating groups affecting addition. Classical (Hammett/Taft) LFERs describe a limited set of molecules: The effect of a substituent on k_R is constant, independent of reaction partner.[17] Instead, our universal LFER applies ΔG values embedding properties of both reaction partners, allowing for wider implementation.[14] We demonstrated evaluating radical reactivity ($^3O_2$, $CO_3^{\bullet -}$, $CH_3^{\bullet}$ etc.) of potentially 100,000+ molecules relevant for many reactions and (metabolic) pathways in environmental science (photolysis/advanced oxidation with O_3) and biology/toxicology ($O_2^{\bullet -}$).[63]

ACKNOWLEDGEMENTS

This work is part of the research programme TTW financing the Contaminants of Emerging Concern in the Water Cycle (CERCEC) Project Number 15759, which is financed by the Dutch Research Council (NWO).

CONFLICT OF INTEREST

The authors declare that they have no conflicts of interest.

DATA AVAILABILITY STATEMENT

The data that support the findings of this study are available in the supporting information of this article.

ORCID

Tom M. Nolte https://orcid.org/0000-0001-8083-0749

ENDNOTE

* When k_{obs} is pH dependent, ΔG needs to incorporate proton shifts (e.g., elimination of $OOH^{\bullet}$ constitutes a net HA by O_2, only assuming peroxynitrite is deprotonated does the data fit the model). See SI3.

REFERENCES

[1] T. M. Nolte, T. Nauser, L. Gubler, *Phys. Chem. Chem. Phys.* **2020**, *22*(8), 4516.
[2] S. K. Pagirea, O. Reiser, *Green Chem.* **2017**, *19*, 1721.
[3] T. M. Nolte, A. M. J. Ragas, *Environmental Science-Processes & Impacts* **2017**, *19*(3), 221.
[4] F. D. Coms, *Proton Exchange Membrane Fuel Cells 8, Pts 1 and 2* **2008**, *16*(2), 235.
[5] J. Holcman, Formation and reactions of radical cations of substituted benzenes in aqueous media. A pulse radiolysis study, in *Risø-M*, **1977**.
[6] E. N. Sharp, P. Rupper, T. A. Miller, *Phys. Chem. Chem. Phys.* **2008**, *10*(27), 3955.
[7] A. J. Hendriks, *Environ. Sci. Technol.* **2013**, *47*(8), 3546.
[8] ECHA, *ECHA's REACH 2018 Roadmap*, Helsinki, Finland **2015**.
[9] C. J. van Leeuwen, J. L. M. Hermens, Properties of chemicals and estimation methodologies, in *Risk assessment of chemicals: An introduction*, Springer **1995** 261.
[10] B. J. Lynch, D. G. Truhlar, *J. Phys. Chem. A* **2001**, *105*(13), 2936.
[11] S. M. Senkan, *Advances in Chemical Engineering* **1992**, *18*, 95.
[12] E. Rosta, A. Warshel, *J. Chem. Theory Comput.* **2012**, *8*(10), 3574.
[13] A. Pross, *Theoretical and physical principles of organic reactivity*, Wiley, New York **1995**.
[14] S. S. Shaik, *Pure Appl. Chem.* **1991**, *63*(2), 195.
[15] S. S. Shaik, P. C. Hiberty, Curve crossing diagrams as general models for chemical reactivity and structure, in *Theoretical treatment of large molecules and their interactions*, Springer-Verlag, Berlin Heidelberg **1991**.
[16] P. R. Wells, *Linear free energy relationships*, Academic P, London, New York **1968** 116.
[17] L. P. Hammett, *J. Am. Chem. Soc.* **1937**, *59*, 96.
[18] C. Hansch, A. Leo, R. W. Taft, *Chem. Rev.* **1991**, *91*(2), 165.
[19] T. M. Nolte, T. Nauser, L. Gubler, A. J. Hendriks, W. J. G. M. Peijnenburg, *PCCP* **2020**, *22*(40), 23215.
[20] S. Fukuzumi, J. K. Kochi, *J. Am. Chem. Soc.* **1981**, *103*(24), 7240.
[21] NIST. *NDRL/NIST solution kinetics database on the web*. **2002**.
[22] G. C. Vogel, R. S. Drago, *J. Chem. Educ.* **1996**, *73*(8), 701.
[23] R. Hardeland, *Biomedical Journal of Scientific & Technical Research* **2017**, *1*(3), 634.
[24] E. Illés, A. Mizrahi, V. Marks, D. Meyerstein, *Free Radic. Biol. Med.* **2019**, *1*(131), 1.
[25] G. Klopman, *Current Contents/Engineering Technology & Applied Sciences* **1984**, *20*, 16.
[26] A. I. Dragan, C. M. Read, C. Crane-Robinson, *Eur. Biophys. J.* **2017**, *46*(4), 301.

[27] K. Matyjaszewski, T. P. Davis, Chapter 1. Theory of radical reactions, in *Handbook of radical polymerization*, Wiley-Interscience, Hoboken **2002**.

[28] J. P. Wagner, M. A. Bartlett, W. D. Allen, M. A. Duncan, *ACS Earth Space Chem.* **2017**, *1*(6), 361.

[29] J. J. P. Stewart, *MOPAC*, Stewart Computational Chemistry, Colorado Springs, CO, USA **2016**.

[30] J. J. P. Stewart, *J. Mol. Model.* **2013**, *19*(1), 1.

[31] M. J. Kamlet, J. L. M. Abboud, M. H. Abraham, R. W. Taft, *J. Org. Chem.* **1983**, *48*(17), 2877.

[32] F. Würthner, *J. Org. Chem.* **2021**.

[33] H. Lin, B. Jin, *Materials* **2010**, *3*, 4214.

[34] Innovest Strategic Value Advisors, I, *Overview of the chemicals industry. Overview for coming clean*. March, New York **2007**.

[35] USEPA, *EPA Office of Compliance Sector Notebook Project. Profile of the Organic Chemical Industry*, Washington, DC 20460 **1995**.

[36] European Chemical Industry Council, *Facts and figures 2017 of the European chemical industry*, Vol. 2017, European Chemical Industry Council, Brussels **2017**, 6.

[37] M. Alsheikhly, *Radiat. Phys. Chem.* **1994**, *44*(3), 297.

[38] T. M. Nolte, W. J. G. M. Peijnenburg, *Environ. Chem.* **2018**, *14*(7), 442.

[39] P. M. Morse, *Phys. Rev.* **1929**, *34*(1), 57.

[40] T. M. Nolte, W. J. G. M. Peijnenburg, *Free Radic. Res.* **2018**, *52*, 1118.

[41] L. H. Jing, J. J. Nash, H. I. Kenttamaa, *J. Am. Chem. Soc.* **2008**, *130*(52), 17697.

[42] F. De Vleeschouwer, V. Van Speybroeck, M. Waroquier, P. Geerlings, F. De Proft, *Org. Lett.* **2007**, *9*(14), 2721.

[43] E. J. Rohwer, M. Akbarimoosavi, S. E. Meckel, X. Liu, Y. Geng, L. M. Lawson Daku, A. Hauser, A. Cannizzo, S. Decurtins, R. J. Stanley, S. X. Liu, T. Feurer, *J. Phys. Chem. C* **2018**, *122*(17), 9346.

[44] C. D. Wright, *Eur. J. Philos. Sci.* **2012**, *2*(375–394), 375.

[45] N. Santschi, T. Nauser, *ChemPhysChem* **2017**, *18*(21), 2973.

[46] H. Y. Chen, S. Jang, T. R. Jinn, J. Y. Chang, H. F. Lu, F. Y. Li, *Chem. Cent. J.* **2012**, *6*.

[47] H. Herrmann, T. Schaefer, A. Tilgner, S. A. Styler, C. Weller, M. Teich, T. Otto, *Chem. Rev.* **2015**, *115*(10), 4259.

[48] G. Klopman, *J. Am. Chem. Soc.* **1968**, *90*, 223.

[49] L. Salem, *J. Am. Chem. Soc.* **1968**, *90*, 543.

[50] D. Rodríguez, A. Rodríguez, A. Notario, A. Aranda, Y. Diaz-de-Mera, E. Martínez, *Atmos. Chem. Phys.* **2005**, *5*, 3433.

[51] X. Fang, X. Pan, A. Rahmann, H. P. Schuchmann, C. von Sonntag, *Chem. Eur. J.* **1995**, *1*(7), 423.

[52] D. J. Henry, M. L. Coote, R. Gómez-Balderas, L. Radom, *J. Am. Chem. Soc.* **2004**, *126*(6), 1732.

[53] M. W. Wong, A. Pross, L. Radom, *Special Issue: Computational Quantum Chemistry - A Cornerstone of Chemical Research (Part B)* **1993**, *33*.

[54] T. Zytowski, H. Fischer, *J. Am. Chem. Soc.* **1996**, *118*(2), 437.

[55] H. Loman, M. Ebert, *Int. J. Radiat. Biol. Relat. Stud. Phys. Chem. Med.* **1970**, *18*(4), 369.

[56] K. Sobańska, A. Krasowska, T. Mazur, K. Podolska-Serafin, P. Pietrzyk, Z. Sojka, *Top. Catal.* **2015**, *58*(12-13), 796.

[57] M. Huang, Z. Wang, L. Hao, W. Zhao, X. Liu, B. Long, L. Fang, *Journal of Molecular Structure-Theochem* **2008**, *862*(1-3), 28.

[58] G. Ghigo, G. Tonachini, *J. Am. Chem. Soc.* **1998**, *120*(27), 6753.

[59] N. Narita, T. Tezuka, *J. Am. Chem. Soc.* **1982**, *104*(25), 7316.

[60] G. Litwinienko, K. U. Ingold, *Acc. Chem. Res.* **2007**, *40*, 222.

[61] R. N. Butler, W. J. Cunningham, A. G. Coyne, L. A. Burke, *J. Am. Chem. Soc.* **2004**, *126*(38), 11923.

[62] R. Koch, R. Knispel, M. Elend, M. Siese, C. Zetzsch, *Atmos. Chem. Phys.* **2007**, *7*(8), 2057.

[63] T. M. Nolte, W. J. G. M. Peijnenburg, T. J. H. M. van Bergen, A. J. Hendriks, *Green Chem.* **2020**, *22*(11), 3558.

[64] T. Umschlag, H. Herrmann, *Acta Hydroch. Hydrob.* **1999**, *27*, 214.

[65] S. Chen, M. Z. Hoffman, G. H. Parsons, *J. Phys. Chem.* **1975**, *79*(18), 1911.

[66] G. E. Adams, R. L. Willson, *Trans. Faraday Soc.* **1969**, *65*(563p), 2981.

[67] J. H. Baxendale, A. A. Khan, *Int. J. Radiat. Phys. Chem.* **1969**, *1*(1), 11.

[68] X. Pan, M. N. Schuchmann, C. vonvon Sonntag, *J. Chem. Soc., Perkin Trans.* **1993**, *2*, 289.

[69] X. Pan, C. von Sonntag, *Z. Naturforsch.* **1990**, *45b*, 1337.

[70] D. Minakata, S. P. Mezyk, J. W. Jones, B. R. Daws, J. C. Crittenden, *Environ. Sci. Technol.* **2014**, *48*(23), 13925.

[71] J. Mönig, K. D. Asmus, M. Schaeffer, T. F. Slater, R. L. Willson, *J. Chem. Soc., Perkin Trans.* **1983**, *2*, 1133.

[72] M. Lal, C. Schöneich, J. Mönig, K. D. Asmus, *Int. J. Radiat. Biol.* **1988**, *54*, 773.

[73] M. H. Abraham, P. L. Grellier, J. L. M. Abboud, R. M. Doherty, R. W. Taft, *Can. J. Chem.* **1988**, *66*, 2673.

[74] L. Valgimigli, J. T. Banks, K. U. Ingold, J. Lusztyk, *J. Am. Chem. Soc.* **1995**, *117*(40), 9966.

[75] *OECD guidelines for the testing of chemicals, Section 1: Physical-chemical properties no. 107: Partition coefficient (n-octanol/water): Shake flask method*, OECD Editions **1995**.

[76] C. L. Tebes-Stevens, W. J. Jones, *Environ. Toxicol. Chem.* **2004**, *23*(7), 1600.

[77] B. Cercek, *J. Phys. Chem.* **1968**, *72*(11), 3832.

[78] M. N. Schuchmann, C. von Sonntag, *J. Phys. Chem.* **1979**, *83*(7), 780.

[79] G. Mark, M. N. Schuchmann, H. P. Schuchmann, C. von Sonntag, *J. Photochem. Photobiol., A* **1990**, *55*, 157.

[80] C. A. Taatjes, *J. Phys. Chem. A* **2006**, *110*(13), 4299.

[81] R. V. Otkjær, H. H. Jakobsen, C. M. Tram, H. G. Kjaergaard, *J. Phys. Chem. A* **2018**, *122*(43), 8665.

[82] J. Seravalli, M. Kumar, W. P. Lu, S. W. Ragsdale, *Biochemistry* **1995**, *34*(24), 7879.

[83] M. P. Bradshaw, C. Barril, A. C. Clark, P. D. Prenzler, G. R. Scollary, *Crit. Rev. Food Sci. Nutr.* **2011**, *51*(6), 479.

[84] B. H. Bielski, H. W. Richter, P. C. Chan, *Ann. N. Y. Acad. Sci.* **1975**, *258*, 231.

[85] L. Zhang, H. M. Muchall, G. H. Peslherbe, *Photochem. Photobiol.* **2013**, *89*(3), 536.

[86] M. Carlsson, M. Jonsson, D. Stenman, T. Reitberger, *J. Wood Chem. Technol.* **2007**, *23*(1), 47.

[87] H. Neugebauer, F. Bohle, M. Bursch, A. Hansen, S. Grimme, *J. Phys. Chem. A* **2020**, *124*(35), 7166.
[88] J. H. Jensen, C. J. Swain, L. Olsen, *J. Phys. Chem. A* **2017**, *121*(3), 699.
[89] W. Shoombuatong, P. Prathipati, W. Owasirikul, A. Worachartcheewan, S. Simeon, N. Anuwongcharoen, J. E. Wikberg, C. Nantasenamat, in *Challenges and advances in computational chemistry and physics. Advances in QSAR Modeling Applications in Pharmaceutical, Chemical, Food, Agricultural and Environmental Sciences*, (Ed: J. Leszczynski), Springer **2017**.
[90] P. O. Dral, O. A. von Lilienfeld, W. Thiel, *J. Chem. Theory Comput.* **2015**, *11*(5), 2120.

SUPPORTING INFORMATION

Additional supporting information may be found in the online version of the article at the publisher's website.

How to cite this article: T. M. Nolte, A. J. Hendriks, L. A. Novák, W. J. G. M. Peijnenburg, *J Phys Org Chem* **2022**, e4317. https://doi.org/10.1002/poc.4317